Supplemental material legends

Supplemental Table S1. Clinical characteristics of enrolled dogs. * Mean and median values are not listed for the "Other neoplasia of bone" category, as only two dogs were enrolled in this group.

Supplemental Table S2. Machine learning algorithms classified post-treatment osteosarcoma samples as either "osteosarcoma – detected" or "osteosarcoma – not detected". Prediction summaries of post-treatment samples (test set) by KNN, BAG, RF, and EXT machine learning models.

Supplemental Figure 1. Exosome production by osteosarcoma cells is positively correlated with tumor progression. (A) Representative images from exosome specific staining in human osteosarcoma tissues. Brown staining indicates positive detection of exosomes. (B) Tissue biopsy samples from human osteosarcoma patients were stained for the presence of exosome markers CD9 and CD63. Box and whisker plots indicate the IHC expression level of the two exosome markers across stage I, II, and III osteosarcomas.

Supplemental Figure 2. Exosome production by osteosarcoma cells is positively correlated with tumor aggressiveness. Cultured dog osteosarcoma cell lines, OSCA-32 and OSCA-40, were stained for tetraspanins CD63, CD9, and CD81 that are enriched in exosomes.

Supplemental Figure 3. Physical and biochemical characterization of osteosarcoma exosomes. (A) Scanning electron micrographs of OSCA-40 exosomes (B) Immunoblotting of exosome preparations documenting enrichment of tetraspanins (CD63) and depletion of β-actin in OSCA-8, OSCA-32, OSCA-40, and OSCA-78 dog osteosarcoma cell lines. (C) NanoSight particle tracking analysis of triplicate samples each of osteosarcoma cell lines OSCA-8, OSCA-32, OSCA-40, and OSCA-78, showing modal diameters of approximately 130 nm.

Supplemental Figure 4. Physical characterization of serum exosomes. NanoSight particle tracking analysis of triplicate samples serum from healthy control (A) and osteosarcoma-positive (B) representative dogs showing modal diameters of approximately 130 nm.

Supplemental Figure 5. Osteosarcoma exosome uptake by fibroblasts and endothelial cells. (A) A CD81-GFP fusion vector was stably transfected into OSCA40 canine osteosarcoma cells. Expression of the fusion protein (green) was determined via confocal immunofluorescent microscopy. Blue staining is the nucleus. (B & C) CD81-GFP tagged exosomes were purified from OSCA40 cells and added to primary cultures of human pulmonary fibroblasts (B) or human pulmonary endothelial cells **(**C**)**. Images of the GFP fluorescence were taken at 0, 1, 2, 4, 8, and 24 hours post treatment with the exosomes. (D & E) Histogram illustrating temporal changes in the number of GFP positive fibroblast and endothelial cells.

Supplemental Figure 6. Osteosarcoma exosomes affect target gene signatures, and increase migration and proliferation of endothelial cells and fibroblasts. (A) Migration of endothelial cells and fibroblasts in a 2D assay compared to control after exposure to osteosarcoma exosomes from OSCA-32 and OSCA-40 cell lines. (B) Proliferation of endothelial cells and fibroblasts in a 2D assay compared to control after exposure to osteosarcoma exosomes from OSCA-32 or OSCA-40 cell lines. (C) qPCR analysis of human fibroblast cells treated with exosomes from OSCA-32 or OSCA-40 cell lines. Data shown are genes whose expression changed relative to control by more than 2-fold.

Supplemental Figure 7. Cell cycle pathways are identified as being associated with differentially expressed host genes. Top networks identified by Ingenuity® Pathway Analysis as being associated with differentially expressed host (mouse) genes.

Supplemental Figure 8. Genes identified in xenografts were validated in canine serum-derived exosomes. Gene expression analysis of (A) SKA2, (B) NEU1, (C) PAF1, (D) PSMG2, and (E) NOB1 gene transcripts by qRT-PCR. Relative expression data were mean centered and scaled to the standard deviation across all samples for each gene. (F) Table showing ANOVA values, demonstrating the relative contribution of each gene transcript to the overall gene signature.

Supplemental Figure 9. Machine learning models comparison based on repeated stratified 10-fold cross-validation analysis of the LDA-transformed training set. (A) Classification accuracy of the Healthy group by KNN, BAG, RF, and EXT learning models based on cross-validation analysis. (B) Representative prediction summary of the training set by the top four machine learning models (KNN, BAG, RF, and EXT) based on a 10-fold cross-validation.

Figure 10. Machine learning performance after data randomization based on repeated 10-fold cross-validations. (A) Original data. (B) Randomized data. (C) Sample distribution was equalized by adding 100 of simulated data points to each group. (D) Randomized equalized data. T-test analysis was performed between original and randomized data. *$p = 0.049$; ***$p < 0.0001$

Supplemental Table S1

		Osteosarcoma (n=28)	Non-neoplastic disease (n=10)	Other neoplasia of bone (n=2)	No apparent disease (n=13)
Breed	Golden retriever	n=6	n=1		
	Labrador retriever	n=3	n=1	n=1	n=4
	Greyhound	n=3	n=1		
	Doberman	n=2			
	Great Dane	n=2			
	German Shepherd				n=2
	Other purebred	n=6	n=6		n=4
	Mixed breed	n=6	n=1	n=1	n=3
Tumor location	Humerus	n=8			
	Radius	n=7		n=1	
	Ulna	n=2			
	Femur	n=2	n/a	n=1	n/a
	Tibia	n=7			
	Fibula	n=1			
	Mandible	n=1			
Sex	Intact female	n=1			
	Spayed female	n=15	n=7		n=6
	Intact male		n=1		n=1
	Castrated male	n-12	n=2	n=2	n=6
Age (years)	Mean	7.2	10.6		6.1
	Median	7.4	11.0		4.8
	Range	2.3 - 11.0	7.0 - 14.0	3.1, 11.1*	2.3 - 14.3
Body weight (kg)	Mean	39.0	30.3		29.8
	Median	34.3	29.7		26.7
	Range	19.5 - 72.0	16.0 - 46.3	31.2, 35.0*	14.9 - 45.0
Time between pre- and post-tx samples (days)	Mean	162			
	Median	39	n/a	n/a	n/a
	Range	2 - 984			
	n/a	n=5			
Non-osteosarcoma disease	Benign splenic lesion		n=5		
	Lipoma	n/a	n=2	n/a	n/a
	Other benign lesion		n=3		
Non-osteosarcoma neoplasia of bone	Metastatic carcinoma	n/a	n/a	n=1	n/a
	Hemangiosarcoma			n=1	

Supplemental Table S1. Clinical characteristics of enrolled dogs. * Mean and median values are not listed for the "Other neoplasia of bone" category, as only two dogs were enrolled in this group.

Supplemental Table S2

Sample	Diagnosis	Post-treatment classification	Days till relapse
Dog 01	Osteosarcoma	Osteosarcoma - NOT detectable	518
Dog 07	Osteosarcoma	Osteosarcoma - detectable	244
Dog 11	Osteosarcoma	Osteosarcoma - NOT detectable	74
Dog 13	Osteosarcoma	Osteosarcoma - NOT detectable	465
Dog 14	Osteosarcoma	Osteosarcoma - detectable	215
Dog 15	Osteosarcoma	Osteosarcoma - NOT detectable	252
Dog 16	Osteosarcoma	Osteosarcoma - NOT detectable	286
Dog 17	Osteosarcoma	Osteosarcoma - detectable	98
Dog 20	Osteosarcoma	Osteosarcoma - NOT detectable	77
Dog 23	Osteosarcoma	Osteosarcoma - NOT detectable	168
Dog 26	Osteosarcoma	Osteosarcoma - NOT detectable	57
Dog 29	Osteosarcoma	Osteosarcoma - NOT detectable	472
Dog 32	Osteosarcoma	Osteosarcoma - NOT detectable	722
Dog 35	Osteosarcoma	Osteosarcoma - detectable	98
Dog 36	Osteosarcoma	Osteosarcoma - detectable	287
Dog 37	Osteosarcoma	Osteosarcoma - detectable	991
Dog 38	Osteosarcoma	Osteosarcoma - detectable	309
Dog 39	Osteosarcoma	Osteosarcoma - detectable	149
Dog 42	Osteosarcoma	Osteosarcoma - detectable	103
Dog 45	Osteosarcoma	Osteosarcoma - detectable	76
Dog 48	Osteosarcoma	Osteosarcoma - NOT detectable	681
Dog 49	Osteosarcoma	Osteosarcoma - detectable	663
Dog 50	Osteosarcoma	Osteosarcoma - detectable	15
Dog 53	Osteosarcoma	Osteosarcoma - detectable	66

Supplemental Table S2. Machine learning algorithms classified post-treatment osteosarcoma samples as either “osteosarcoma – detected” or “osteosarcoma – not detected”. Prediction summaries of post-treatment samples (test set) by KNN, BAG, RF, and EXT machine learning models.

Supplemental Figure 1

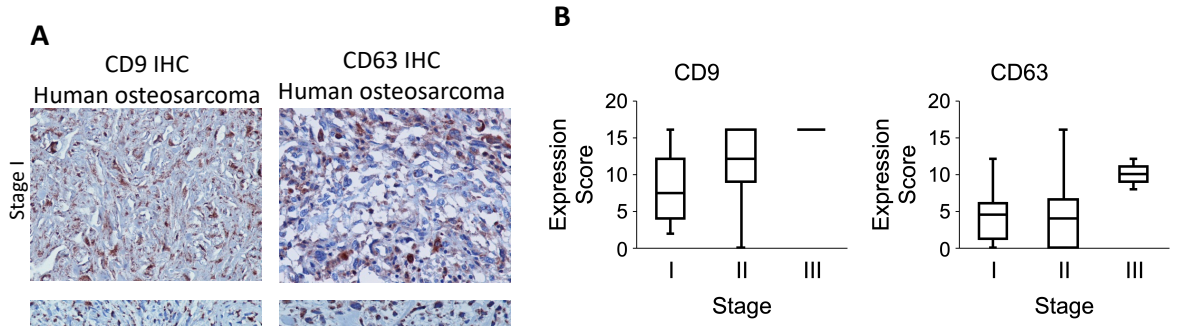

Supplemental Figure 1. Exosome production by osteosarcoma cells is positively correlated with tumor progression. (A) Representative images from exosome specific staining in human osteosarcoma tissues. Brown staining indicates positive detection of exosomes. (B) Tissue biopsy samples from human osteosarcoma patients were stained for the presence of exosome markers CD9 and CD63. Box and whisker plots indicate the IHC expression level of the two exosome markers across stage I, II, and III osteosarcomas.

Supplemental Figure 2

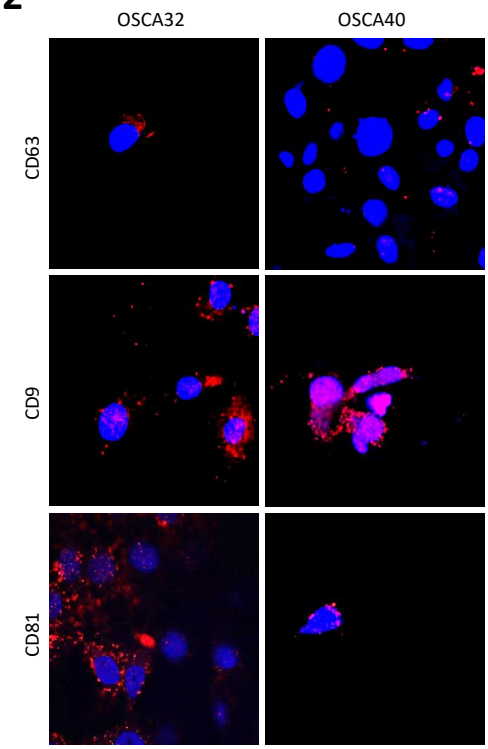

Supplemental Figure 2. Exosome production by osteosarcoma cells is positively correlated with tumor aggressiveness. Cultured dog osteosarcoma cell lines, OSCA-32 and OSCA-40, were stained for tetraspanins CD63, CD9, and CD81 that are enriched in exosomes.

Supplemental Figure 3

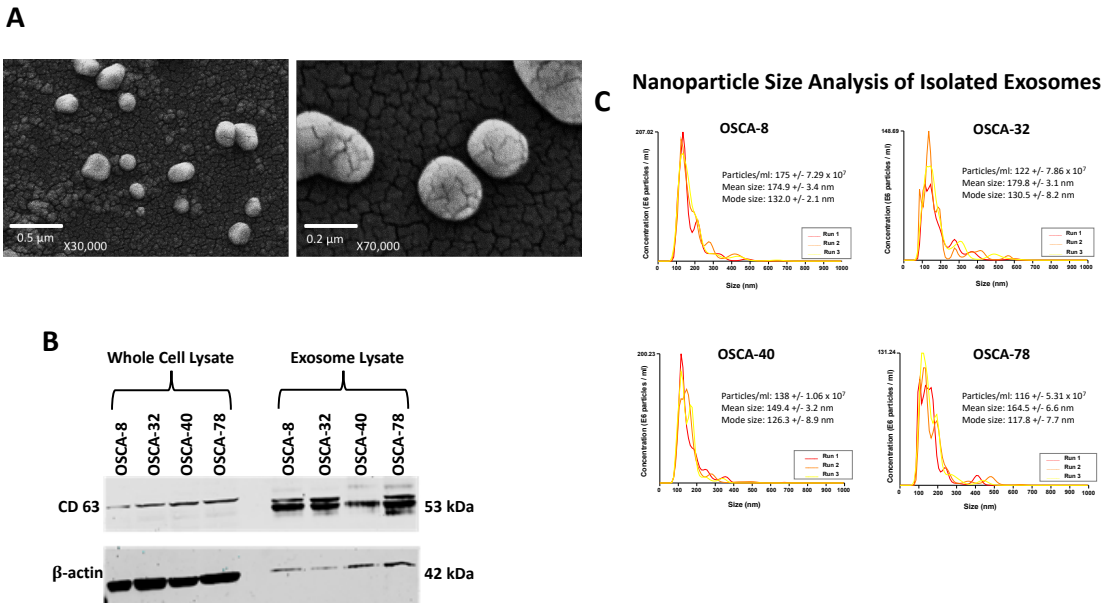

Supplemental Figure 3. Physical and biochemical characterization of osteosarcoma exosomes. (A) Scanning electron micrographs of OSCA-40 exosomes (B) Immunoblotting of exosome preparations documenting enrichment of tetraspanins (CD63) and depletion of β-actin in OSCA-8, OSCA-32, OSCA-40, and OSCA-78 dog osteosarcoma cell lines. (C) NanoSight particle tracking analysis of triplicate samples each of osteosarcoma cell lines OSCA-8, OSCA-32, OSCA-40, and OSCA-78, showing modal diameters of approximately 130 nm.

Supplemental Figure 4

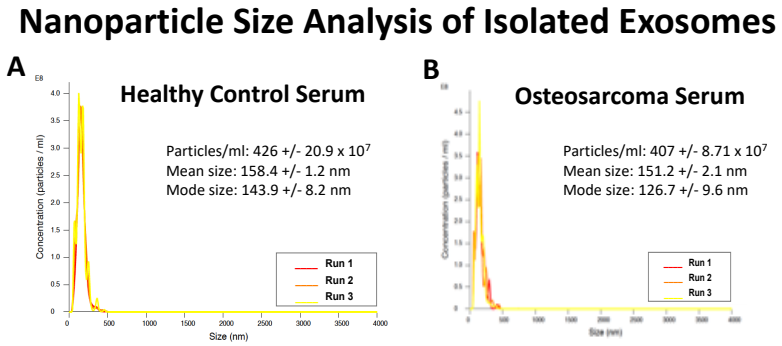

Supplemental Figure 4. Physical characterization of serum exosomes. NanoSight particle tracking analysis of triplicate samples serum from healthy control (A) and osteosarcoma-positive (B) representative dogs showing modal diameters of approximately 130 nm.

Supplemental Figure 5

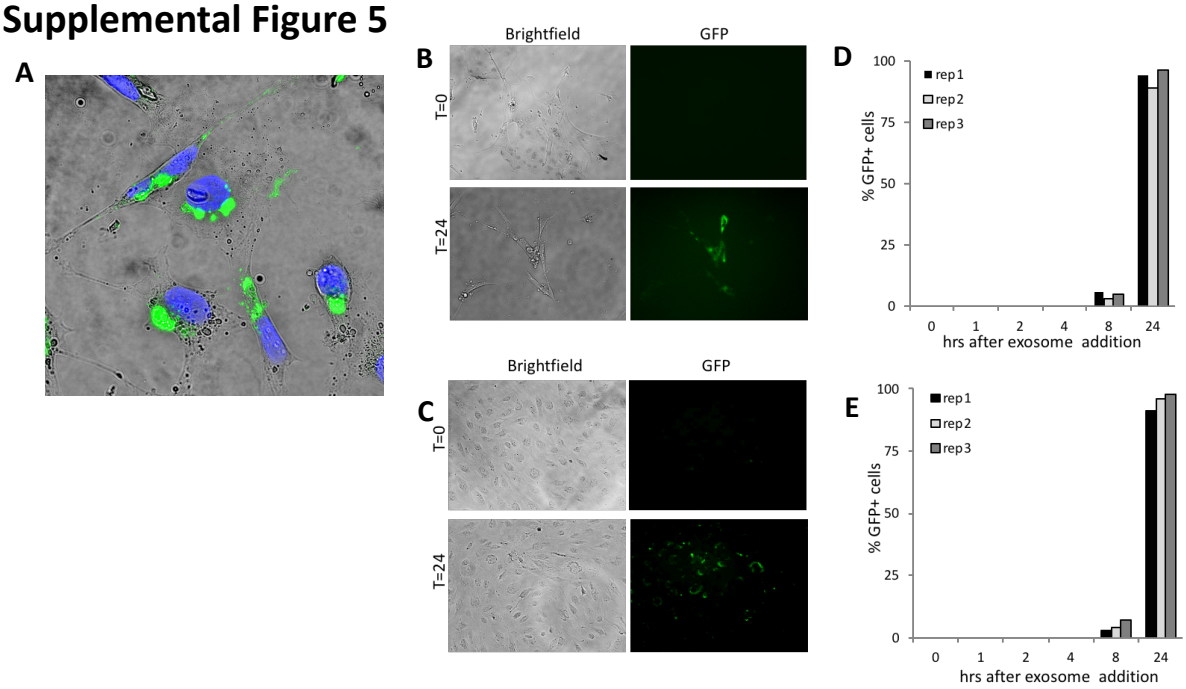

Supplemental Figure 5. Osteosarcoma exosome uptake by fibroblasts and endothelial cells. (A) A CD81-GFP fusion vector was stably transfected into OSCA40 canine osteosarcoma cells. Expression of the fusion protein (green) was determined via confocal immunofluorescent microscopy. Blue staining is the nucleus. (B & C) CD81-GFP tagged exosomes were purified from OSCA40 cells and added to primary cultures of human pulmonary fibroblasts (B) or human pulmonary endothelial cells **(**C**)**. Images of the GFP fluorescence were taken at 0, 1, 2, 4, 8, and 24 hours post treatment with the exosomes. (D & E) Histogram illustrating temporal changes in the number of GFP positive fibroblast and endothelial cells.

Supplemental Figure 6

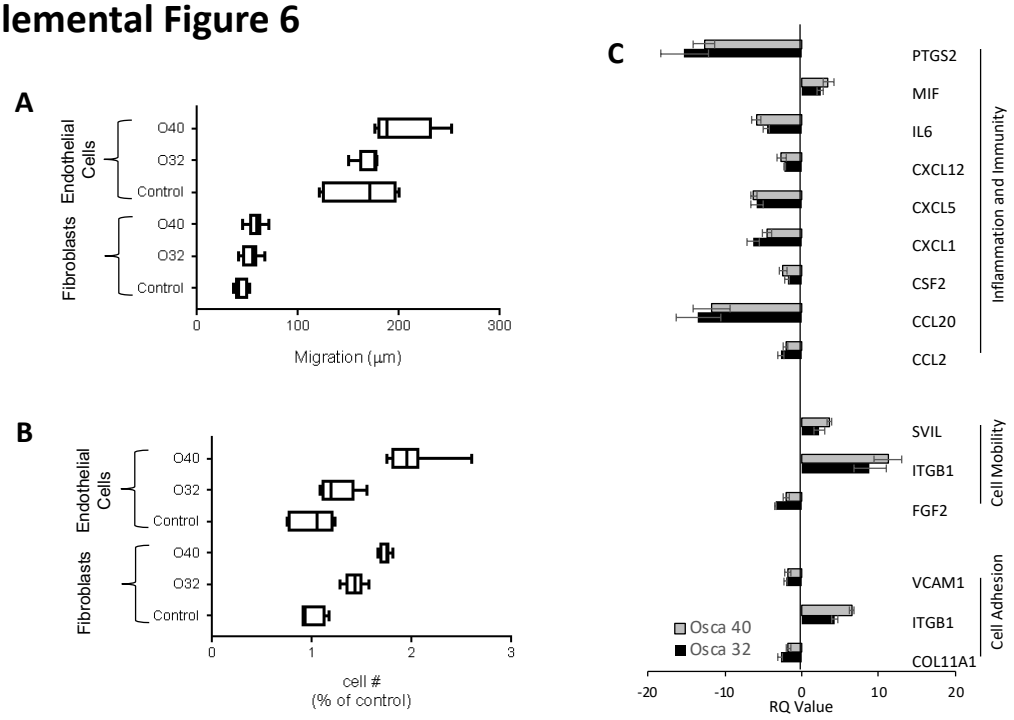

Supplemental Figure 6. Osteosarcoma exosomes affect target gene signatures, and increase migration and proliferation of endothelial cells and fibroblasts. (A) Migration of endothelial cells and fibroblasts in a 2D assay compared to control after exposure to osteosarcoma exosomes from OSCA-32 and OSCA-40 cell lines. (B) Proliferation of endothelial cells and fibroblasts in a 2D assay compared to control after exposure to osteosarcoma exosomes from OSCA-32 or OSCA-40 cell lines. (C) qPCR analysis of human fibroblast cells treated with exosomes from OSCA-32 or OSCA-40 cell lines. Data shown are genes whose expression changed relative to control by more than 2-fold.

Supplemental Figure 7

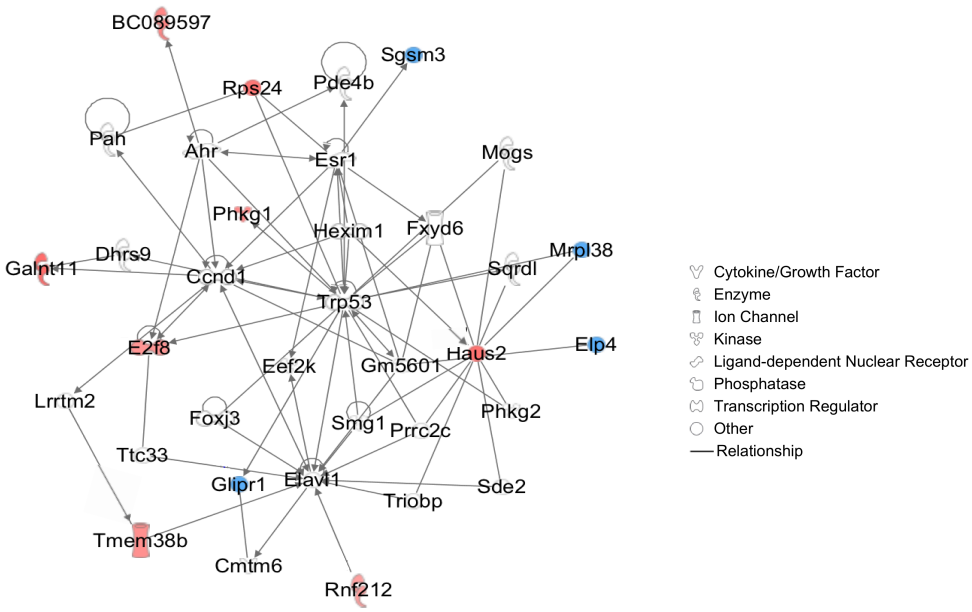

Supplemental Figure 7. Cell cycle pathways are identified as being associated with differentially expressed host genes. Top networks identified by Ingenuity® Pathway Analysis as being associated with differentially expressed host (mouse) genes.

Supplemental Figure 8

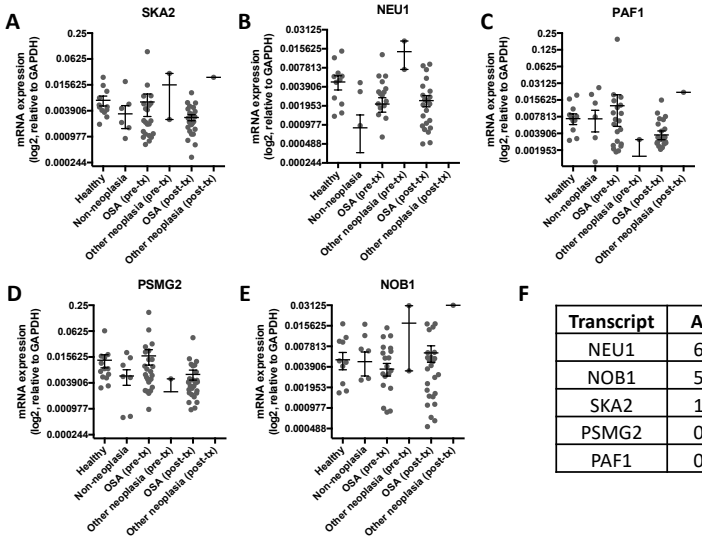

F

Transcript	ANOVA
NEU1	6.9971
NOB1	5.7371
SKA2	1.6257
PSMG2	0.4215
PAF1	0.0071

Supplemental Figure 8. Genes identified in xenografts were validated in canine serum-derived exosomes. Gene expression analysis of (A) SKA2, (B) NEU1, (C) PAF1, (D) PSMG2, and (E) NOB1 gene transcripts by qRT-PCR. Relative expression data were mean centered and scaled to the standard deviation across all samples for each gene. (F) Table showing ANOVA values, demonstrating the relative contribution of each gene transcript to the overall gene signature.

Supplemental Figure 9

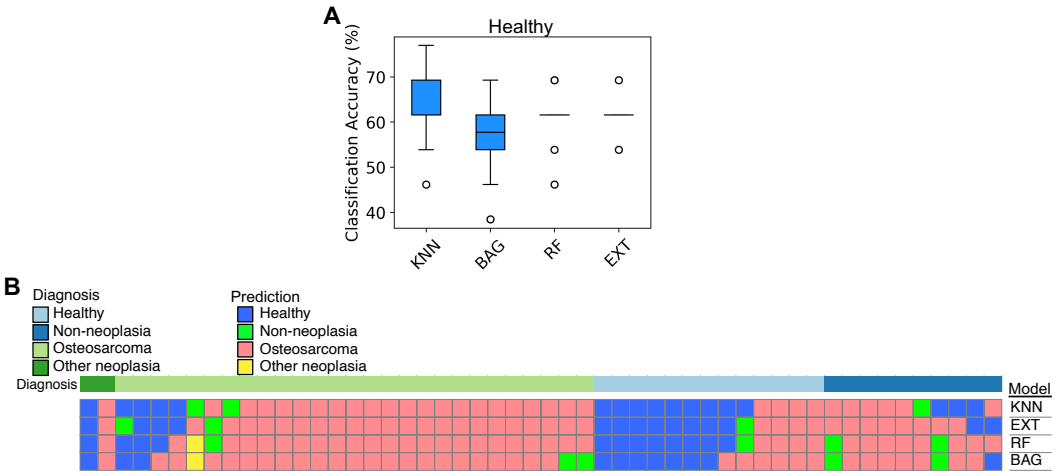

Supplemental Figure 9. Machine learning models comparison based on repeated stratified 10-fold cross-validation analysis of the LDA-transformed training set. (A) Classification accuracy of the Healthy group by KNN, BAG, RF, and EXT learning models based on cross-validation analysis. (B) Representative prediction summary of the training set by the top four machine learning models (KNN, BAG, RF, and EXT) based on a 10-fold cross-validation.

Supplemental Figure 10

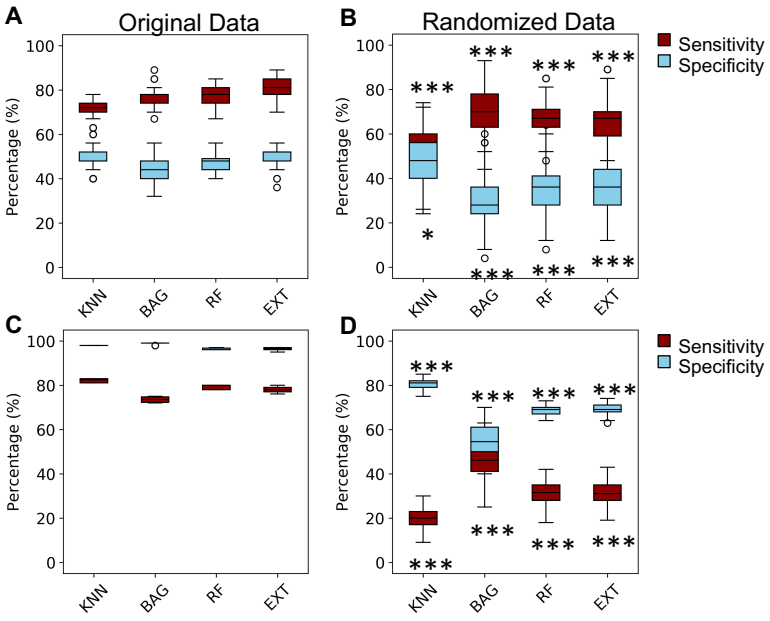

Figure 10. Machine learning performance after data randomization based on repeated 10-fold cross-validations. (A) Original data. (B) Randomized data. (C) Sample distribution was equalized by adding 100 of simulated data points to each group. (D) Randomized equalized data. T-test analysis was performed between original and randomized data. *p = 0.049; ***p < 0.0001